Journal of Physics B: Atomic, Molecular and Optical Physics

PAPER

Measurements of linear polarization of satellite transitions from Li- and Be-like Ar ions

To cite this article: A C Gall *et al* 2020 *J. Phys. B: At. Mol. Opt. Phys.* **53** 145004

IOP Publishing Journal of Physics B: Atomic, Molecular and Optical Physics
J. Phys. B: At. Mol. Opt. Phys. **53** (2020) 145004 (9pp) https://doi.org/10.1088/1361-6455/ab8eff

Measurements of linear polarization of satellite transitions from Li- and Be-like Ar ions

A C Gall[1], Dipti[2], S W Buechele[2], S Sanders[3], C I Szabo[2,4], R Silwal[2,3], Yu Ralchenko[2], N Brickhouse[1] and E Takacs[2,3]

[1] Harvard-Smithsonian Center for Astrophysics, 60 Garden Street, Cambridge, MA 02138, United States of America
[2] National Institute of Standards and Technology, Gaithersburg, MD 20899, United States of America
[3] Department of Physics and Astronomy, Clemson University, Clemson, SC 29634, United States of America
[4] Theiss Research, 7411 Eads Ave, La Jolla, CA 92037, United States of America

E-mail: amy.gall@cfa.harvard.edu

Received 18 March 2020, revised 20 April 2020
Accepted for publication 30 April 2020
Published 18 June 2020

Abstract

Non-thermal electron distributions, such as beams of electrons, are found in many laboratory and astrophysical plasma sources and can produce anisotropic and polarized emission. Theories used to model the emission require sublevel specific analysis, which can be difficult to verify experimentally. Using two polarization-sensitive Johann-type crystal spectrometers at the National Institute of Standards and Technology (NIST) electron beam ion trap facility, we measured the linear polarization of well-known dielectronic recombination satellite transitions from Li-like Ar ions and two blended features from Be-like ions. The spectrometers observed the plasma at 90° relative to the electron beam propagation direction, and the crystal dispersion planes were oriented perpendicular relative to each other to allow for differing polarization sensitivities. Measurements were taken near the resonance energies of each line and compared with theoretical predictions based on relativistic magnetic sublevel atomic kinetics using the density-matrix theory. Most of the predictions are in excellent agreement with measured values.

Keywords: polarization, spectroscopy, highly-charged ions, electron beam ion trap, magnetic sublevels, x-rays

(Some figures may appear in colour only in the online journal)

1. Introduction

Physical properties of astrophysical and laboratory plasmas are often determined from spectral observations aided by theoretical models. Inferring accurate information from spectra requires a reliable knowledge of the ionization balance and a detailed understanding of the atomic processes occurring. One such process, dielectronic recombination (DR), can be the dominant recombination process that plays a vital role in determining the equilibrium conditions of hot collisional plasmas. The radiationless first step of DR occurs when a continuum electron is captured by a recombining ion, while a bound atomic electron is simultaneously excited. As the ion relaxes from the doubly excited state to the ground state of the recombined ion through a single or multiple radiative decays, the DR process is complete. The required matching of the kinetic energy (KE) of the initial continuum electron plus the binding energy of the captured electron with the excitation energy of the core electron makes DR a resonant process occurring only with electrons of selected KE

in the plasma. Since DR occurs at electron energies below the direct excitation (DE) threshold of the parent line, the ratio of unblended satellite lines to strong DE lines samples different regions of the electron energy distribution and can be a powerful diagnostic of plasma temperature (see e.g. [1–4]).

An electron beam ion trap (EBIT), well suited for systematic atomic studies due to the variety of accessible elements and the tuneable quasi mono-energetic electron beam that allows for a degree of charge state and excitation selectivity, is an ideal device for studying DR and producing atomic data such as DR cross sections [5–7]. The emission produced in an EBIT originates from ions excited by a uni-directional electron beam, rather than an isotropic electron distribution. Therefore, the emitted radiation can be anisotropic and linearly polarized [8]. Anisotropic and polarized emission is also observed in astrophysical sources such as solar flares (see e.g. [9–12]), where beams of electrons travel along magnetic field lines. The polarization of discrete line emission originates from non-statistically populated magnetic sublevels created by processes such as electron impact excitation (EIE) or recombination (radiative or dielectronic). Therefore, to accurately diagnose non-thermal plasmas it is important to use reliable, sublevel specific, theories verified by experiment. The controlled and relatively simple plasma environment created by EBITs is ideal for polarization measurements needed to benchmark various theoretical approaches used to calculate sublevel specific cross sections (see e.g. [13–15]).

While the majority of EBIT polarization studies have focused on emission following EIE, there have also been a few measurements of polarized emission from states populated by dielectronic capture. For example, Shlyaptseva *et al* [16, 17] calculated the polarization-dependent spectra of DR satellite lines from the B and Be-like charge states of Fe and compared with experimental EBIT spectra measured with two von Hámos spectrometers. Jörg *et al* [18] used an EBIT and the Compton polarimetry technique to measure the linear polarization of Li- and Be-like satellite transitions in Xe ions and showed that some of the transitions are sensitive to the Breit interaction [19]. Using a similar setup, Shah *et al* [20] reported the linear polarization of x-ray emission following the DR process in He- through O-like charge states of Kr and further demonstrated sensitivity of the polarization to the Breit interaction. Later, Shah *et al* [21] used two identical solid-state Ge detectors located at 0° and 90° relative to the electron beam propagation direction to observe emission asymmetries from K-shell satellite lines of He- through O-like charge states of Fe.

Adding to this collection of studies, we report measurements and a theoretical analysis of linear polarizations of strong Li-like Ar satellites including the j, k, a, r, q, and blended $t + s$ line (in the notation of [4]). We also report the polarizations from two measured blended features resulting from Be-like Ar transitions. In the sections that follow, the details of our experimental procedure are discussed, and our experimental results are presented. Theoretical polarization values calculated with the flexible atomic code (FAC) [22] are also explained and compared with experimental results.

2. Experimental procedure

2.1. Experimental setup

Measurements were taken at the EBIT facility at the National Institute of Standards and Technology (NIST). The vertically oriented NIST EBIT has been described extensively in previous works (see, e.g. [23]), but relevant details are discussed here. In short, the EBIT is a cylindrically symmetric system used to create and trap ions for spectroscopic study. The main components of the device include the electron gun (e-gun), drift tube (trap), and collector assemblies. A quasi mono-energetic electron beam emanates from a barium-doped, 3 mm diameter, curved cathode in the e-gun with currents up to 150 mA. As the beam travels vertically upwards towards the trap, it is compressed to approximately a 35 μm radius and $10^{11}\mathrm{cm}^{-3}$ density by a superconducting magnet capable of producing an up to 2.7 T field.

The trap consists of three cylindrical drift tube electrodes capable of floating up to 30 kV voltage with up to 500 V difference between the electrodes. Neutral atoms or low charge state ions are injected into the trapping region, where they interact with the electron beam and become ionized through electron impact ionization. Ions are electrostatically trapped in the axial direction by the relative voltages placed on the three drift tube electrodes. For our measurements the upper drift tube was set to +250 V above the middle drift tube (MDT) voltage and the lower drift tube was set to +500 V above the MDT. Every 5 s the middle drift tube voltage is raised to +400 V for 10 ms to dump the ions. The space charge of the electron beam and the shape of the electrodes provide additional radial trapping of the ions. The space charge offset (e.g. [24, 25]), estimated by comparing experimental and theoretical DR resonance beam energies, was found to be about 90 eV for the energies and currents used in this work.

Defining the direction of the electron beam as the quantization axis, observations were made at 90° with respect to this axis. Measurements were taken simultaneously with two crystal spectrometers with CCD detectors capable of resolving features less than 2 eV apart at 3 keV x-ray energy. Both crystal spectrometers housed a Si(111) crystal with 6.271 Å interplanar spacing (2d value from [26]). One of the crystal spectrometers was oriented with the crystal's plane of dispersion perpendicular to the electron beam, while the second spectrometer was rotated so that the plane of dispersion was oriented parallel with the electron beam. These are henceforth referred to as horizontal and vertical spectrometer orientations, respectively (see figure 1).

Measurements were taken in a steady-state mode, where the electron beam energy and current remain constant during measurements. In addition to improving the signal to noise ratio, this mode allows the charge state balance to reach the steady-state equilibrium. Since it takes a fraction of a second to reach steady-state equilibrium, and given our trapping and collection times are 5 s and minutes long, respectively, the steady state approximation is justified. The two crystal spectrometers were set to reflect 3114 eV x-ray photons at the center of the spectrum. With a bandwidth of roughly 120 eV, the spectrometers

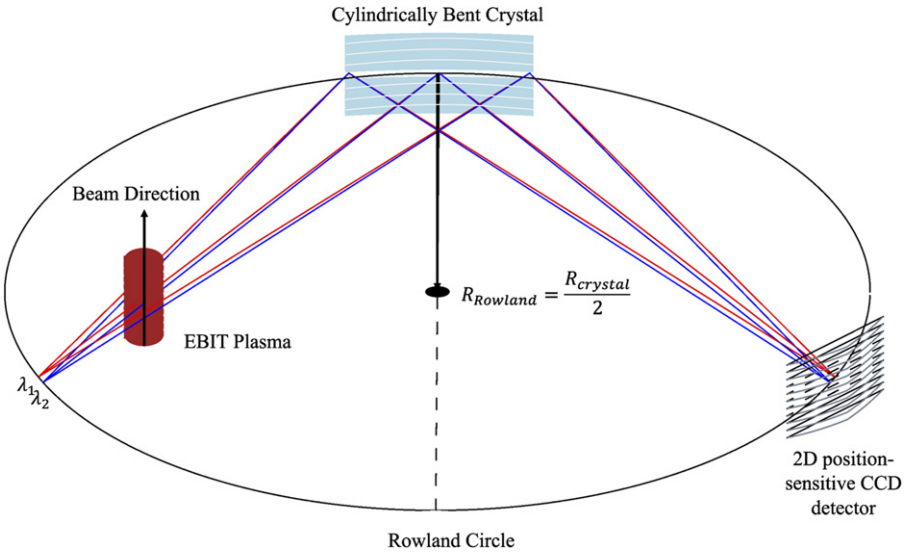

Figure 1. Schematic showing the orientation of the cylindrically bent crystal, electron beam, and Rowland circle for the horizontal spectrometer orientation. In the vertical orientation the crystal, Rowland circle, and CCD are rotated 90° in the counterclockwise direction.

measured photon energies ranging from 3054 eV to 3174 eV and covered the KLL (in inverse Auger notation) DR satellite transitions of interest.

Measurements were first taken at an off-resonance electron beam energy of 3.87 keV and an electron beam current of 128.5 mA for calibration purposes. Emission from the He-like resonance $1s^2\,{}^1S–1s2p\,{}^1P$, intercombination $1s^2\,{}^1S–1s2p\,{}^3P$, and forbidden $1s^2\,{}^1S–1s2s\,{}^3S$ transitions were measured in 3 min intervals for a total collection time of about 40 min.

KLL satellite transitions were measured by finely scanning the electron beam energy from 2.16 keV to 2.29 keV in 10 eV increments to cover the resonance energies of all of the strong Li-like satellite transitions of our interest. The electron beam current was kept constant at 74 mA while measurements were taken for 12–18 min at each beam energy setting.

2.2. Polarization of the emission from the EBIT plasma

For our experimental setup, the linear polarization of the observed emission is defined as:

$$P = \frac{I_{\parallel} - I_{\perp}}{I_{\parallel} + I_{\perp}} \tag{1}$$

where $I_{\parallel}$ and $I_{\perp}$ are the polarization components of the intensity defined by the electric field direction parallel and perpendicular to the quantization axis, respectively. Both of the crystal spectrometers preferentially reflect x-rays polarized perpendicular to the crystal's plane of dispersion. Therefore, the two crystal orientations provide different polarization sensitivities that allow us to determine both polarization components. The measured intensity for the vertical (I_{vert}) and horizontal (I_{hor}) orientations can be expressed as:

$$I_{\mathrm{vert}} = \Omega_{\mathrm{v}}\eta_{\mathrm{v}}\left[RI_{\parallel} + I_{\perp}\right], \tag{2}$$

$$I_{\mathrm{hor}} = \Omega_{\mathrm{h}}\eta_{\mathrm{h}}\left[I_{\parallel} + RI_{\perp}\right], \tag{3}$$

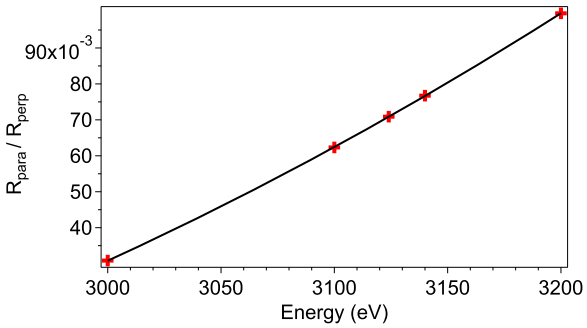

Figure 2. Calculated ratio of integrated crystal reflectivities at photon energies near DR lines of interest. Values calculated with XOP shown as markers. Third order polynomial fit shown as solid line.

where $\eta_{\mathrm{v,h}}$ is the detection efficiency and $\Omega_{\mathrm{v,h}}$ is a factor that includes the geometry with solid angle of acceptance for the vertical and horizontal spectrometers, respectively [3]. $R_{\parallel}$ and $R_{\perp}$ are the integrated crystal reflectives for x-rays polarized parallel and perpendicular to the plane of dispersion, and the ratio (R) is defined as $R = \frac{R_{\parallel}}{R_{\perp}}$.

Values for R may be estimated by $R = |\cos^m(2\theta)|$, where $1 \leqslant m \leqslant 2$ and θ is the Bragg angle. The limits of m correspond to perfect ($m = 1$) and mosaic ($m = 2$) crystals, while real crystals typically have R values between the two limits. The R values used for our work were calculated using the x-ray oriented program (XOP) software [27] for a range of Bragg angles, including angles corresponding to 3000 eV, 3100 eV, 3124 eV, 3140 eV, and 3200 eV photon energies. A third order polynomial was fit to these data points to extract the R value for each measured line (shown in figure 2).

Given the vertical slit-like shape of the EBIT source, the effective source size is different for the two spectrometer orientations [28]. To account for differences in geometry and efficiency, the spectrometers were normalized to one another using an unpolarized line (the Li-like m line, see section 2.3) as

a reference. By using the same crystal in both spectrometers, the normalization factor (N) reduces to the ratio of the geometrical factors and efficiencies, allowing $I_{\rm vert}$ to be expressed in terms of $\Omega_{\rm h}\eta_{\rm h}$. The measured polarization may then be defined in terms of the measured intensities, the normalization factor, and the ratio of the crystal reflectives:

$$P = \frac{(1+R)}{(1-R)}\frac{(I_{\rm hor} - NI_{\rm vert})}{(I_{\rm hor} + NI_{\rm vert})}. \quad (4)$$

2.3. Experimental analysis and results

The data collected by the CCDs included contributions from diffracted x-rays, electronic readout noise, cosmic rays, and thermal noise. Energy and spatial discrimination techniques outlined in [29] were used to filter the data and improve the signal to noise ratio. Additional procedures were used to process the data from the vertical spectrometer, as the crystal/source geometry at this orientation produces shape alterations of the diffracted lines. The line curvatures produced were systematically fit and straightened to reduce the broadening. We describe the details of this procedure in our recent work [30].

All spectral peaks and background were simultaneously fit using weighted fitting tools of a multi-peak fitting software package. In agreement with previous works [13], we found that spectral peaks were primarily Gaussian in shape. As such, Gaussians were fit to each peak and a polynomial function to the background by weighing each data point by its statistical uncertainty, set by the number of counts. The total uncertainties in the line intensities therefore include the statistical uncertainties and uncertainties from the fit.

To reduce the uncertainties in the line positions, particularly for very weak features, spectra were summed to increase the signal to noise ratio. Peak locations obtained by fitting the summed spectra were later used as constraints when fitting the spectra recorded at each electron beam energy. The widths of individual non-blended lines were constrained to be equal in each spectrum. Lower energy peaks resulting from a blend of lines from Be-like ions (see table 2) were left unconstrained due to the uncertainty and variability in the peak location and width.

While a number of unpolarized lines exist in the spectra (see section 3), the Li-like m line [4] was the strongest, well resolved feature suitable for normalization. The normalization factor (N) was determined by taking the ratio of intensities of the m line in the summed (2.25 keV and 2.26 keV) horizontal and vertical spectra. The normalization factor (2.42 ± 0.38) as described above was used to correct the vertical spectra for differences in efficiencies and geometry.

Results from the electron beam energy scan over the KLL resonances are shown in figure 3, where spectra have been corrected for any difference in collection time. The He-like direct excitation features (energies from [31, 32]) measured at 3.87 keV beam energy were used to calibrate the x-ray spectra. The strong Li-like features have been identified and labeled using the notation of [4]. Weak features appearing at lower photon energies and at electron beam energies above 2.22 keV are from blended satellite transitions in Be-like ions.

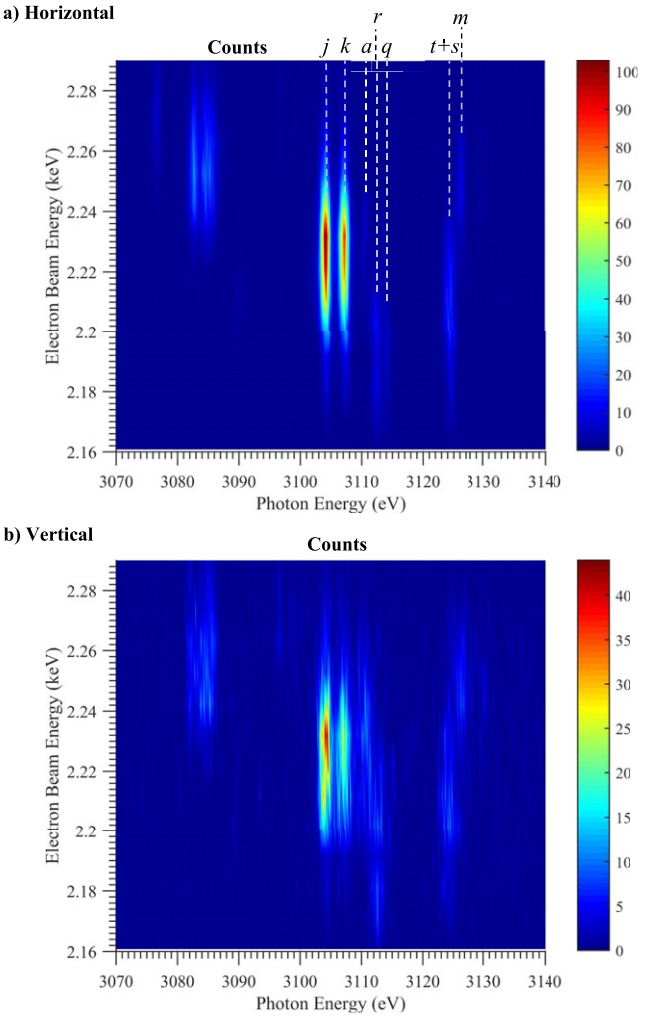

Figure 3. Scan of electron beam energies over KLL resonances. (a) Measured spectra from the horizontally oriented spectrometer. (b) Measured spectra from the vertically oriented spectrometer.

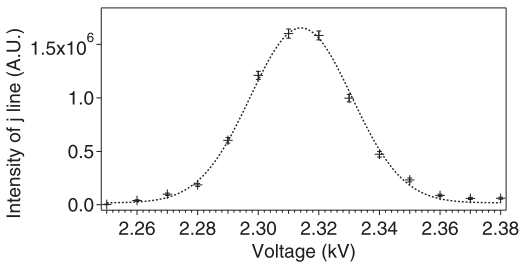

Figure 4. Electron beam energy profile fit with a weighted Gaussian function. X-axis represents the experimental middle drift tube voltage setting, not corrected for space charge effects. Fit FWHM = 0.04 kV, $x_0 = 2.314$ kV.

To quantify the electron beam energy profile and width, the intensity of the j line was measured at each electron beam energy. The line intensity vs. electron beam energy measured with the horizontally oriented spectrometer, shown in figure 4, was fit with a Gaussian function weighted with the statistical uncertainty. The full width at half maximum (FWHM) of the electron beam energy profile was found to be approximately 40 eV in agreement with previous estimates.

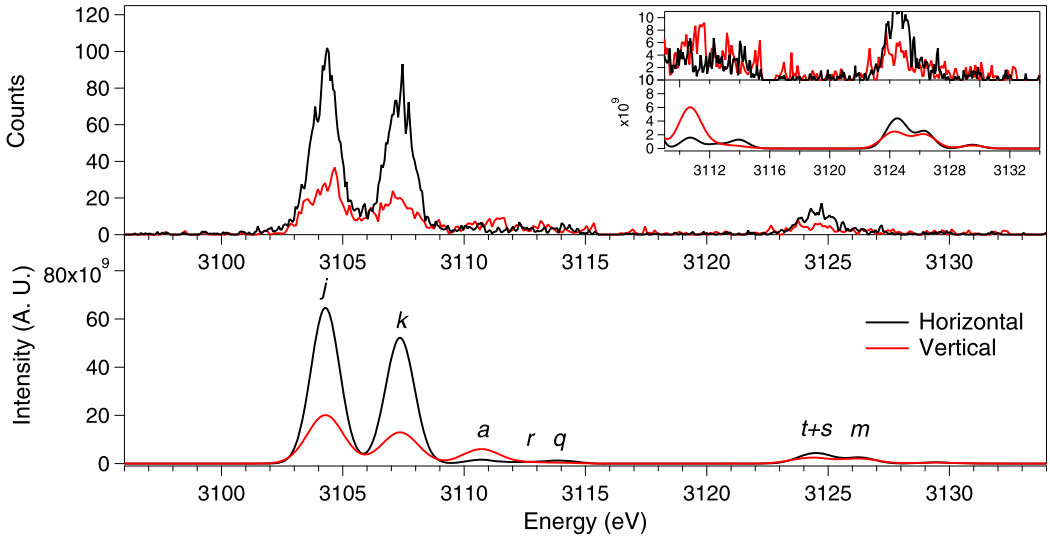

Figure 5. Top panel: experimental spectra from horizontally and vertically oriented spectrometers measured at an electron beam energy near the maximum intensity of the j line. Bottom panel: synthetic spectra with an electron beam energy of 2.22 keV. Top right insert shows $a, r, q, t+s$, and m lines enhanced.

Table 1. Measured and theoretical polarization values. Theoretical polarization values are given for the case of an observation angle of 90° and for observation angles of 90° ± γ, where γ is the pitch angle (see discussion in section 4). Li-like satellite energies from [33] in the notation of [4].

Line	E_{line}(eV)	Transition	E_{AI}(keV)	P_{exp}	P_{FAC}	$P_{\text{FAC}}(90° \pm \gamma)$
u	3088.02	$1s2s2p(^3P^\circ)^4P^\circ_{3/2} \rightarrow 1s^22s\,^2S_{1/2}$	2.17	—	0.60	—
f	3088.21	$1s2p^2(^3P)^4P_{3/2} \rightarrow 1s^22p_{3/2}\,^2P^\circ_{3/2}$	2.21	—	−0.75	—
e	3089.75	$1s2p^2(^3P)^4P_{5/2} \rightarrow 1s^22p_{3/2}\,^2P^\circ_{3/2}$	2.21	—	0.50	—
g	3091.38	$1s2p^2(^3P)^4P_{3/2} \rightarrow 1s^22p_{1/2}\,^2P^\circ_{1/2}$	2.20	—	0.60	—
l	3104.19	$1s2p^2(^1D)^2D_{3/2} \rightarrow 1s^22p_{3/2}\,^2P^\circ_{3/2}$	2.22	—	−0.75	—
j	3104.29	$1s2p^2(^1D)^2D_{5/2} \rightarrow 1s^22p_{3/2}\,^2P^\circ_{3/2}$	2.22	0.46 ± 0.08	0.50	0.47
k	3107.37	$1s2p^2(^1D)^2D_{3/2} \rightarrow 1s^22p_{1/2}\,^2P^\circ_{1/2}$	2.22	0.55 ± 0.08	0.60	0.57
a	3110.71	$1s2p^2(^3P)^2P_{3/2} \rightarrow 1s^22p_{3/2}\,^2P^\circ_{3/2}$	2.23	−0.53 ± 0.28	−0.74	−0.63
r	3112.47	$1s2s2p(^3P^\circ)^2P^\circ_{1/2} \rightarrow 1s^22s\,^2S_{1/2}$	2.19	0.05 ± 0.13	0.00	0.00
b	3113.88	$1s2p^2(^3P)^2P_{3/2} \rightarrow 1s^22p_{1/2}\,^2P^\circ_{1/2}$	2.23	—	0.60	—
q	3114.14	$1s2s2p(^3P^\circ)^2P^\circ_{3/2} \rightarrow 1s^22s\,^2S_{1/2}$	2.20	0.47 ± 0.27	0.60	0.57
$t+s$ blend	3124.13	t: $1s2s2p(^1P^\circ)^2P^\circ_{1/2} \rightarrow 1s^22s\,^2S_{1/2}$	2.21	0.25 ± 0.11	0.25	0.21
	3124.80	s: $1s2s2p(^1P^\circ)^2P^\circ_{3/2} \rightarrow 1s^22s\,^2S_{1/2}$	2.21			
m	3126.35	$1s2p^2(^1S)^2S_{1/2} \rightarrow 1s^22p_{3/2}\,^2P^\circ_{3/2}$	2.24	0.00 ± 0.17	0.00	0.00

The spectra measured at 2.22 keV electron beam energy, where the j line is close to its maximum measured value, are shown in figure 5 (top panel). The j and k lines measured with the horizontal spectrometer are much stronger than those measured with vertical, indicating a large, positive polarization. The spectra show that the $t+s$ blended line also has a positive polarization, while the a line has a negative polarization. As a verification of our normalization, the r line, which is fundamentally unpolarized, has roughly equal intensities in both spectra.

The polarization values for the j, k, r, q, a, m, and $t+s$ blend are given in table 1 (P_{exp}) along with their calculated autoionization energies (E_{AI}). The polarization values were measured at the electron beam energy corresponding to the maximum intensity of each line or, in the case of blended lines, where each line was best resolved.

The blended Be-like satellite lines, measured around 2.26 keV beam energy, are seen at energies between 3074–3090 eV in figure 6 (top panel). The measured polarization values for the two blends are given in table 2. The low counts measured by the vertical spectrometer and highly blended features made fitting difficult and limited the number of usable peaks. As a result, the experimental polarization values listed in table 2 may not include some unaccounted systematic uncertainties.

3. Theoretical approach

The total intensity of lines produced by a beam of electrons observed at 90° relative to the beam direction is given by:

$$I(90^\circ) = I_{\parallel} + I_{\perp}. \tag{5}$$

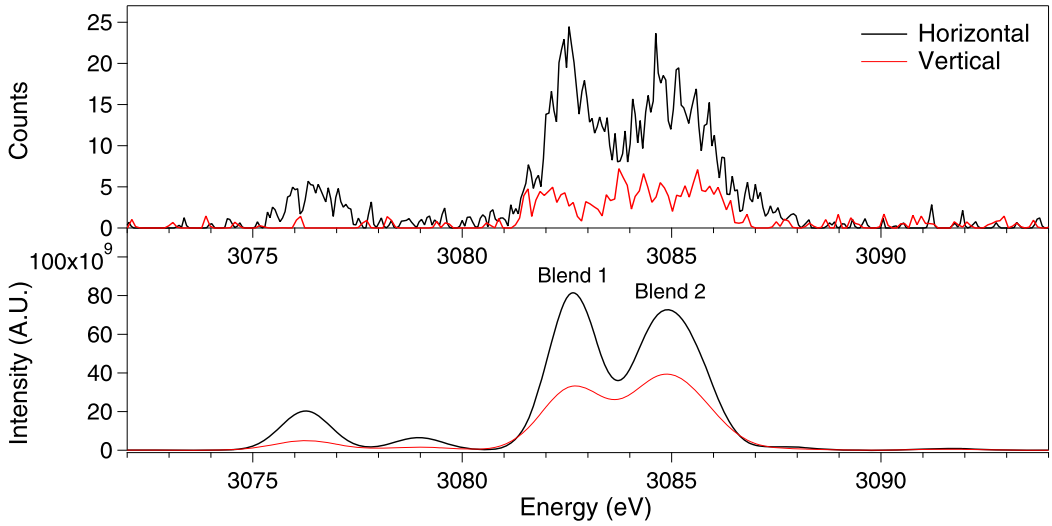

Figure 6. Top panel: experimental spectra from horizontally and vertically oriented spectrometers taken at an electron beam energy near the maximum intensity of the strongest Be-like features. Bottom panel: synthetic spectra with an electron beam energy of 2.26 keV.

Using the formula describing the angular dependence of dipole radiation given in [8], $I(90^\circ)$ is related to the 4π-averaged intensity $\langle I\rangle$ by:

$$I(90^\circ) = \langle I\rangle \frac{3}{3-P}. \tag{6}$$

By combining equations (1), (5) and (6), the polarization components of the intensity can be expressed in terms of the 4π-averaged intensity:

$$I_\perp = \frac{3}{2}\langle I\rangle \frac{(1-P)}{(3-P)} \tag{7}$$

$$I_\parallel = \frac{3}{2}\langle I\rangle \frac{(1+P)}{(3-P)}. \tag{8}$$

Following the procedure of [16], $\langle I\rangle$ can be written in terms of the intensity factor Q_d ([35]), the electron energy distribution function $f(E)$, and the autoionization energy $E_{\rm AI}$. For this experiment, as previously discussed, the electron energy distribution is characterized by a Gaussian function centered at the beam energy $E_{\rm b}$ with a FWHM of $\Delta E = 40$ eV.

$$I_\perp = \frac{3}{2}\frac{Q_d}{\Delta E}\sqrt{\frac{4\ln 2}{\pi}}\exp\left[-4\ln 2\left(\frac{E_{\rm b}-E_{\rm AI}}{\Delta E}\right)^2\right]\frac{(1-P)}{(3-P)} \tag{9}$$

$$I_\parallel = \frac{3}{2}\frac{Q_d}{\Delta E}\sqrt{\frac{4\ln 2}{\pi}}\exp\left[-4\ln 2\left(\frac{E_{\rm b}-E_{\rm AI}}{\Delta E}\right)^2\right]\frac{(1+P)}{(3-P)} \tag{10}$$

The theoretical polarization (P) values used in equations (9) and (10) were calculated within the photon density matrix formalism (see e.g. [16, 36–39]). Within the electric dipole approximation, the degree of polarization of the DR lines, observed at an angle θ relative to the electron beam, can be expressed as follows [38, 39]:

$$P = \frac{-\frac{3}{2}A_{20}G_2(\alpha_{id}J_{id},\alpha_f J_f)\sin^2\theta}{1+A_{20}G_2(\alpha_{id}J_{id},\alpha_f J_f)P_2(\cos\theta)} \tag{11}$$

where A_{20} and G_2 are the alignment parameter and the structure function, respectively. $P_2(\cos\theta)$ is the second order Legendre polynomial. The normalized alignment parameter A_{20} describes the non-statistical population distribution among magnetic sublevels of the upper level and is given as

$$A_{20} = \frac{\sqrt{(2J_{id}+1)}}{\sigma(\alpha_{id}J_{id})}\Sigma_{M_{id}}(-1)^{J_{id}-M_{id}}\langle J_{id}M_{id}J_{id}-M_{id}|20\rangle\,\sigma(\alpha_{id}J_{id}M_{id}) \tag{12}$$

where J, M, and α denote the total angular momentum, its corresponding magnetic component, and all other quantum numbers required to describe the state, respectively. For the dielectronic recombination process, the initial state of the ion (prior to e^- capture), the intermediate doubly excited state, and the final state (after photon emission) are characterized by subscripts i, id, and f, respectively. $\langle J_{id}M_{id}J_{id}-M_{id}|20\rangle$ in equation (12) represents the Clebsch–Gordan coefficient, $\sigma(\alpha_{id}J_{id}M_{id})$ is the cross section for dielectronic capture of the substate with magnetic quantum number M, and $\sigma(\alpha_{id}J_{id})$ is the total dielectronic capture cross section.

The structure function G_2, which reflects the angular momentum coupling between the intermediate doubly excited and the final states, can be expressed as

$$G_2(\alpha_{id}J_{id},\alpha_f J_f) = (-1)^{(1+J_{id}+J_f)}\begin{Bmatrix}1 & 1 & 2\\ J_{id} & J_{id} & J_f\end{Bmatrix}\sqrt{\frac{3(2J_{id}+1)}{2}} \tag{13}$$

where the quantity in curly brackets denotes the Wigner 6j-symbol.

As an example, from table 1, the k, q, and s lines all have $J_{id} = 3/2$ and $J_f = 1/2$ values. Solving for the alignment parameter and structure function, the final expression for the degree of polarization at an observation angle of 90° for this transition reduces to a combination of the cross sections for dielectronic capture of the substate with magnetic quantum number M_{id}:

$$P(90^\circ) = 3\,\frac{\sigma(1/2)-\sigma(3/2)}{5\sigma(1/2)+3\sigma(3/2)}. \tag{14}$$

Table 2. Measured and theoretical polarization values of strong satellite transitions from Be-like ions. Theoretical polarization values are given for the case of an observation angle of 90° and for observation angles of $90° \pm \gamma$, where γ is the pitch angle (see discussion in section 4). Transitions and energies from [34].

Line	E_{line}(eV)	Transition	E_{AI}(keV)	P_{exp}	P_{FAC}	$P_{\text{FAC}}(90° \pm \gamma)$
	3076.27	$1s2s2p^2\ ^1D_2 \rightarrow 1s^22s2p\ ^1P_1$	2.28	—	0.60	—
	3076.53	$1s2s^22p\ ^3P^\circ_1 \rightarrow 1s^22s^2\ ^1S_0$	2.22	—	−1.00	—
	3078.90	$1s2s2p^2\ ^3P_2 \rightarrow 1s^22s2p\ ^1P_1$	2.28	—	0.60	—
Blend 1	3082.41	$1s2s2p^2\ ^3D_2 \rightarrow 1s^22s2p\ ^3P_2$	2.26	0.56 ± 0.13	0.39	0.38
	3082.43	$1s2s2p^2\ ^3P_1 \rightarrow 1s^22s2p\ ^3P_2$	2.26			
	3082.60	$1s2s2p^2\ ^3D_3 \rightarrow 1s^22s2p\ ^3P_2$	2.26			
	3083.87	$1s2s2p^2\ ^3D_1 \rightarrow 1s^22s2p\ ^3P_2$	2.26			
Blend 2	3084.50	$1s2s2p^2\ ^3D_2 \rightarrow 1s^22s2p\ ^3P_1$	2.26	0.58 ± 0.11	0.25	0.22
	3085.40	$1s2s2p^2\ ^3P_1 \rightarrow 1s^22s2p\ ^3P_0$	2.26			
	3085.58	$1s2s2p^2\ ^3P_2 \rightarrow 1s^22s2p\ ^3P_2$	2.26			
	3085.96	$1s2s2p^2\ ^3D_1 \rightarrow 1s^22s2p\ ^3P_1$	2.26			
	3088.65	$1s2s2p^2\ ^1P_1 \rightarrow 1s^22s2p\ ^1P_1$	2.29	—	−0.25	—
	3091.54	$1s2s2p^2\ ^1S_0 \rightarrow 1s^22s2p\ ^1P_1$	2.30	—	0.00	—
	3091.75	$1s2s^22p\ ^1P^\circ_1 \rightarrow 1s^22s^2\ ^1S_0$	2.24	—	0.42	—
	3101.02	$1s2s2p^2\ ^1D_2 \rightarrow 1s^22s2p\ ^3P_2$	2.28	—	−1.00	—

Due to axial symmetry, states having $J_{id} = 1/2$ will have a polarization of zero (see e.g. [11]), therefore the measured m and r lines have zero polarization.

The flexible atomic code (cfac 1.6.1) [22] was used to generate the required atomic data for equations (9)–(11). These data included the energy levels, radiative and autoionization probabilities, and dielectronic capture rates. Unlike Maxwellian plasmas, the quasi mono-energetic electron beam cannot excite any of KLL satellites at their respective resonance energies which are well below the excitation thresholds. Therefore, only dielectronic capture from the ground state of He- and Li-like Ar was considered to populate the doubly excited states of Li- and Be-like ions, respectively. This assumption is generally valid for low density EBIT plasmas, where most of the population is in the ground states of the respective ion stages. Since the measurements were taken at electron beam energies close to the resonance energy of each line, cascades were also not expected to contribute to the populations and were therefore not included in our analysis. The calculated polarization values are listed in tables 1 and 2 (P_{FAC}) along with the experimental values. Non-zero theoretical polarization values for lines that are too weak to experimentally measure are also included in tables 1 and 2.

4. Discussion

From the polarization calculations, the intensities in the parallel and perpendicular polarization modes were calculated using equations (9), and (10). In figures 5 and 6, the theoretical spectra, calculated with an electron beam energy of 2.22 keV and 2.26 keV, respectively, are shown with experimental spectra for comparison. The calculated crystal reflectivites were applied to the theoretical intensity components to produce the synthetic EBIT spectra according to equations (2) and (3). The theoretical spectra, convolved with a Gaussian with FWHM of 1.4 eV and 1.8 eV for the horizontal and vertical spectra, respectively, show strong agreement with our experiment. The j, k, and $t + s$ lines show a positive polarization in both the experimental and synthetic spectra with comparable relative intensities between the horizontal and vertical spectra. Similarly, the a line shows negative polarization in both spectra, while the m and r lines appear unpolarized in both the theoretical and experimental spectra, as expected.

The equations used in our analysis assume that the electrons travel in a single direction along the axis of the EBIT. While a good approximation, this is not physically exact, as electrons follow a spiral path as they interact with the magnetic field. Typically, EBITs are designed to minimize the magnetic field in the electron gun region. This means that as electrons travel from the electron gun (near zero magnetic field) to the trap (2.7 T field), they travel along a converging helical path. As a result, the quantization axis may be rotated from the z-axis (this rotation angle is called the pitch angle), and the observation angle may be off from the assumed 90°. These effects may lead to some depolarization of the observed spectral lines.

To estimate the maximum amount of depolarization, we follow the optical approach developed by Herrmann [40] and verified by Beiersdorfer & Slater [41]. The Herrmann theory shows that the product of the beam area and the transverse temperature is constant. Using this to equate the area and transverse energy ($E_\perp$) at the cathode to the area and transverse energy in the trap, we may calculate $E_\perp$ at the trap as:

$$E_\perp = kT\left(\frac{r_c^2}{r_t^2}\right) \tag{15}$$

where k is the Boltzmann constant, T is the temperature of the cathode, and r_c and r_t are the beam radius at the cathode and trap, respectively. From the transverse energy, the pitch angle (γ) is calculated as

$$\sin^2\gamma = \frac{E_\perp}{E_{\text{beam}}} \tag{16}$$

where E_{beam} is the electron beam energy.

Using $T = 1400$ K (estimated from the filament current and voltage), $r_c = 1.5$ mm (the radius of the cathode), and $r_t = 35$ μm (calculated as in [24]), we find $E_\perp = 222$ eV and $\gamma = 18.4°$ for an electron beam energy of 2.22 keV. We note that the beam radius at the cathode may be as low as 1.0 mm [41], and the beam radius at the trap as low as 25 μm, as the magnetic field at the e-gun is not exactly known. This gives a lower limit estimate of $E_\perp$ of about 100 eV.

From the estimated transverse velocity, the 'true' polarization for dipole transitions may be calculated as [42]:

$$P_0 = \frac{2P}{2 - \frac{E_\perp}{E_{\text{beam}}}(3 - P)} \tag{17}$$

where P_0 is the polarization for the case when $E_\perp = 0$ (observation angle of 90°), and P is the measured polarization.

Using equation (11), we calculated the theoretical polarization at an observation angle of $90° \pm \gamma$ (using the maximum γ of 18.4°) for direct comparison to our measurements. These results are listed in tables 1 and 2 as P_{FAC} $(90° \pm \gamma)$ and show excellent agreement with the measured values, giving us confidence in our estimated value for γ. All of the Li-like transitions fall within our experimental uncertainties, with the largest deviations for the a and q lines. Figure 3 and table 1 show that the resonance energies of the r and q lines are less than 2 eV apart, making it difficult to clearly separate the two. Similarly, the a line has very weak contributions from the d line. Without contributions from the d line, the a line has a polarization of $P_{\text{FAC}} = -0.75$. In both cases (with and without inclusion of the d line) however $P_{\text{FAC}}(90° \pm \gamma) = -0.63$, demonstrating that the pitch angle (γ) causes a reduction in the theoretical polarization which must be accounted for.

The theoretical Be-like spectra generally reproduce the measured spectra. As previously mentioned, some minor disagreements seen between our measured and theoretical polarization values for Be-like transitions are likely due to the low counts and large number of blended features.

5. Conclusions

Using the two-crystal method, we report the measured linear polarization of satellite transitions from Li-like and Be-like Ar. The comparison between experimental and theoretical spectra in figures 5 and 6 shows an overall agreement. This is further seen in table 1, where all theoretical predictions fall within the experimental uncertainties. Taking experimental depolarization effects into account shifts the theoretical values slightly lower, where an even better agreement is found.

Acknowledgments

This work was partially funded by the NIST Grant Award Numbers 70NANB16H204, 70NANB18H284, and 70NANB19H024 of the Measurement Science and Engineering (MSE) Research Grant Programs, by the NASA/GFSC Grant Award Number 80NSSC18K0234, and by the National Science Foundation Award Number 1806494.

ORCID iDs

A C Gall https://orcid.org/0000-0002-8260-2229
Dipti https://orcid.org/0000-0001-6675-8509
C I Szabo https://orcid.org/0000-0002-6125-7948
Yu Ralchenko https://orcid.org/0000-0003-0083-9554
N Brickhouse https://orcid.org/0000-0002-8704-4473
E Takacs https://orcid.org/0000-0002-2427-5362

References

[1] Beiersdorfer P, Hell N and Lepson J K 2018 *Astrophys. J* **864** 24
[2] Savin D W, Beiersdorfer P, Kahn S M, Beck B R, Brown G V, Gu M F, Liedahl D A and Scofield J H 2000 *Rev. Sci. Instrum.* **71** 3362–72
[3] Biedermann C, Radtke R and Fournier K B 2002 *Phys. Rev.* E **66** 066404
[4] Gabriel A H 1972 *Mon. Not. R. Astron. Soc.* **160** 99–119
[5] Knapp D A, Marrs R E, Schneider M B, Chen M H, Levine M A and Lee P 1993 *Phys. Rev.* A **47** 2039–46
[6] McLaughlin D J, Hahn Y, Takács E, Meyer E S and Gillaspy J D 1996 *Phys. Rev.* A **54** 2040–9
[7] Gall A C, Foster A R, Silwal R, Dreiling J M, Borovik A, Kilgore E, Ajello M, Gillaspy J D, Ralchenko Y and Takács E 2019 *Astrophys. J* **872** 194
[8] Percival I and Seaton M 1958 *Phil. Trans. R. Soc.* **251** 113–38
[9] Haug E 1979 *Sol. Phys.* **61** 129–42
[10] Akita K, Tanaka K and Watanabe T 1983 *Sol. Phys.* **86** 101–5
[11] Inal M K and Dubau J 1987 *J. Phys. B: At. Mol. Opt. Phys.* **20** 4221–39
[12] Dubau J, Inal M and M Urnov A 1996 *Phys. Scr.* **T65** 179
[13] Takács E *et al* 1996 *Phys. Rev.* A **54** 1342–50
[14] Beiersdorfer P *et al* 1996 *Phys. Rev.* A **53** 3974–81
[15] Nakamura N, Kato D, Miura N, Nakahara T and Ohtani S 2001 *Phys. Rev.* A **63** 024501
[16] Shlyaptseva A S, Mancini R C, Neill P, Beiersdorfer P, Crespo López-Urrutia J R and Widmann K 1998 *Phys. Rev.* A **57** 888–98
[17] Shlyaptseva A S, Mancini R C, Neill P and Beiersdorfer P 1999 *J. Phys. B: At. Mol. Opt. Phys.* **32** 1041–51
[18] Jörg H, Hu Z, Bekker H, Blessenohl M A, Hollain D, Fritzsche S, Surzhykov A, Crespo López-Urrutia J R and Tashenov S 2015 *Phys. Rev.* A **91** 042705
[19] Breit G 1929 *Phys. Rev.* **34** 553–73
[20] Shah C *et al* 2015 *Phys. Rev.* A **92** 042702
[21] Shah C, Amaro P, Steinbrügge R, Bernitt S, López-Urrutia J R C and Tashenov S 2018 *Astrophys. J. Suppl. Ser.* **234** 27
[22] Gu M 2008 *Can. J. Phys.* **86** 675–89
[23] Gillaspy J D 1997 *Phys. Scr.* **T71** 99–103
[24] Levine M A, Marrs R E, Henderson J R, Knapp D A and Schneider M B 1988 *Phys. Scr.* **22** 157–63
[25] Porto J V, Kink I and Gillaspy J D 2000 *Rev. Sci. Instrum.* **71** 3050–8
[26] Henke B, Gullikson E and Davis J 1993 *At. Data Nucl. Data Tables* **54** 181–342
[27] Dejus R J and Sanchez del Rio M 1996 *Rev. Sci. Instrum.* **67** 3356
[28] Henderson J R *et al* 1990 *Phys. Rev. Lett.* **65** 705–8
[29] Hudson L *et al* 2007 *Nucl. Instrum. Methods Phys. Res.* A **580** 33–6
[30] Dipti, Buechele S W, Gall A C, Sanders S C, Szabo C I, Silwal R, Takacs E and Ralchenko Y 2020 *J. Phys. B: At. Mol. Opt. Phys.* **53** 115701

[31] Bruhns H, Braun J, Kubiček K, Crespo López-Urrutia J R and Ullrich J 2007 *Phys. Rev. Lett.* **99** 113001
[32] Saloman E B 2010 *J. Phys. Chem. Ref. Data* **39** 033101
[33] Yerokhin V A and Surzhykov A 2018 *J. Phys. Chem. Ref. Data* **47** 023105
[34] Yerokhin V A, Surzhykov A and Fritzsche S 2015 *Phys. Scr.* **90** 054003
[35] Vainshtein L and Safronova U 1978 *At. Data Nucl. Data Tables* **21** 49–68
[36] Inal M K and Dubau J 1989 *J. Phys. B: At. Mol. Opt. Phys.* **22** 3329–41
[37] Blum K 1996 *Density Matrix Theory and Applications* 2nd edn (New York: Plenum Press)
[38] Balashov V V, Grum-Grzhimailo A N and Kabachnik N M 2000 *Polarization and Correlation Phenomena in Atomic Collisions* (New York: Plenum)
[39] Sharma L, Surzhykov A, Inal M K and Fritzsche S 2010 *Phys. Rev.* A **81** 023419
[40] Herrmann G 1958 *J. Appl. Phys.* **29** 127–36
[41] Beiersdorfer P and Slater M 2001 *Phys. Rev.* E **64** 066408
[42] Gu M F, Savin D W and Beiersdorfer P 1999 *J. Phys. B: At. Mol. Opt. Phys.* **32** 5371–8